

A New Statistical Indicator to Study Nonlinear Gravitational Clustering and Structure Formation

J.S.Bagla^{*} and T.Padmanabhan[†]

Inter-University Centre for Astronomy and Astrophysics, Post Bag 4, Ganeshkhind, Pune 411 007, INDIA

Submitted to MNRAS

ABSTRACT

In an $\Omega = 1$ universe dominated by nonrelativistic matter, velocity field and gravitational force field are proportional to each other in the linear regime. Neither of these quantities evolve in time and these can be scaled suitably so that the constant of proportionality is unity and velocity and force field are equal. The Zeldovich approximation extends this feature beyond the linear regime, until formation of pancakes. Nonlinear clustering which takes place *after* the breakdown of Zeldovich approximation, breaks this relation and the mismatch between these two vectors increases as the evolution proceeds. We suggest that the difference of these two vectors could form the basis for a powerful, new, statistical indicator of nonlinear clustering. We define an indicator called velocity contrast, study its behaviour using N-Body simulations and show that it can be used effectively to delineate the regions where nonlinear clustering has taken place. We discuss several features of this statistical indicator and provide simple analytic models to understand its behaviour. Particles with velocity contrast higher than a threshold have a correlation function which is biased with respect to the original sample. This bias factor is scale dependent and tends to unity at large scales.

Key words: Galaxies : clustering – cosmology : theory – dark matter, large scale structure of the Universe

^{*} E-mail : jasjeet@iucaa.ernet.in

[†] paddy@iucaa.ernet.in

1 INTRODUCTION

Large scale structures like galaxies etc. are believed to have formed out of small density perturbations via gravitational instability. This process, in most popular models, is driven by dark matter which is the dominant constituent of the universe. We can compute rate of growth of clustering using linear theory when the perturbations are small. Linear theory however has a very limited domain of validity and we have to resort to numerical simulations for studying evolution of inhomogeneities at late epochs.

In linear regime density field is related to velocity field in a unique manner [in the growing mode] and the density field alone specifies the system completely. Evolution of perturbations is described by a second order differential equation and specification of initial density field and velocity field completely determine the state of the system at any later time. However for a given nonlinear density field there is no practical method for computing velocity field. Our understanding of nonlinear regime will improve if we have a simple physical indicator of velocity field. We introduce velocity contrast, a new statistical indicator, that may be used to quantify some features of velocity field.

Velocity contrast can be used for comparison of simulation results with observations. It provides a simple and stable algorithm in contrast with some other methods that are used for this purpose. These methods are required as studies of nonlinear gravitational clustering have focussed mainly on aspects relating to dark matter. Comparison of these studies with observations is made difficult by the fact that we observe only sources of light. Many techniques have been devised for isolating regions that can host galaxies in numerical simulations. Some of these are quite elaborate, like DENMAX (Bertschinger and Gelb 1991), and hence computationally very intensive. Other schemes, like density threshold or the friend of friend algorithm are very simple to implement but have problems with interlopers as these algorithms do not use dynamical information. We show that velocity contrast can be used to isolate regions of interest in a relatively simple and robust manner.

In next section, we briefly review dynamical evolution of trajectories in a system undergoing gravitational collapse. This is used to motivate the form of new indicator which is introduced in §3. In §4 we use N-Body simulations to study velocity contrast for CDM and an HDM like spectrum. §5 contains discussion of the new indicator using spherical model and nonlinear approximations. In §6 we compare density and velocity contrast and study

the average relation between them as well as dispersion around it. We also discuss clustering properties of nonlinear mass and with respect of total mass.

2 EVOLUTION OF TRAJECTORIES

The problem of gravitational dynamics in an expanding universe can be simplified considerably for nonrelativistic matter, at scales that are much smaller than hubble radius. In this domain, we can take the newtonian limit of relativistic equations. If mass of the universe is dominated by collisionless matter [e.g. dark matter] then the system is entirely characterised by the following equations :

$$\begin{aligned}
 \frac{d\mathbf{u}}{db} &= -\frac{3}{2} \frac{Q}{b} (\mathbf{u} - \mathbf{g}) \\
 \nabla^2 \psi &= \left(\frac{\delta}{b} \right) \\
 \mathbf{g} &\equiv -\nabla \psi \equiv -\frac{2}{3H_0^2 \Omega_0} \left(\frac{a}{b} \right) \nabla \varphi \\
 Q &= \left(\frac{\rho_b}{\rho_c} \right) \left(\frac{\dot{a}b}{ab} \right)^2
 \end{aligned} \tag{1}$$

where $\mathbf{u} = d\mathbf{x}/db$ is the "velocity" at time t , φ is the gravitational potential due to the perturbed dark matter distribution, \mathbf{g} is the rescaled gravitational force, $a(t)$ is the expansion factor, ρ_b is the background density, ρ_c is the critical density and $b(t)$ is the growing solution to the equation

$$\ddot{b} + \frac{2\dot{a}}{a} \dot{b} = 4\pi G \rho_b b. \tag{2}$$

In a matter dominated universe with $\Omega = 1$, we have $b = a$ and $Q = 1$. [We shall consider only this case here though generalisation of our analysis to other models is straightforward.]

The equations (1) describe a complicated many body system even in the limit of a smooth gravitational potential. From the structure of (1), we can distinguish four different epochs in the evolution of clustering — linear, Zeldovich, quasilinear and nonlinear.

At sufficiently early time $\delta \ll 1$ and we can use linear perturbation theory to study growth of perturbations. In this limit, we can easily solve (1) and show that

$$\begin{aligned}
 \delta(a, \mathbf{x}) &= af(\mathbf{x}) \\
 \mathbf{u}(a, \mathbf{x}) &= u(\mathbf{x}) = \mathbf{g}(\mathbf{x}) \\
 \mathbf{g}(\mathbf{x}) &= -\nabla \psi(\mathbf{x}) \\
 \nabla^2 \psi(\mathbf{x}) &= f(\mathbf{x})
 \end{aligned} \tag{3}$$

Clearly, $\mathbf{u}(a, \mathbf{x})$ and $\mathbf{g}(a, \mathbf{x})$ are independent of a and $\delta \propto a$. Also note that in linear regime, $\mathbf{u}(a, \mathbf{x}) = \mathbf{g}(a, \mathbf{x})$. [Velocity here is, of course, defined in a dynamically relevant manner as $\mathbf{u} = (d\mathbf{x}/da)$; the conventional definition of peculiar velocity is $\mathbf{v} = a\dot{\mathbf{x}} = a\dot{a}\mathbf{u}$ and it scales as $v \propto a\dot{a} \propto a^{1/2}$. We shall work with \mathbf{u} since we can always obtain \mathbf{v} by a simple rescaling.]

Linear theory becomes invalid when density contrast becomes comparable to unity, however we can understand some aspects of dynamics by using the Zeldovich approximation (Zeldovich 1970). This approximation extrapolates equality of velocity and force beyond linear regime.

$$\begin{aligned} \mathbf{u}(a, \mathbf{q}) &= \mathbf{g}(a_{in}, \mathbf{q}) = -\nabla\psi(a_{in}, \mathbf{q}) \\ \mathbf{x} &= \mathbf{q} + b(a)\mathbf{u}(a, \mathbf{q}) \end{aligned} \quad (4)$$

Here \mathbf{q} is initial position of the particle, also called its lagrange position. Particles move with constant velocity \mathbf{u} that is related to the force at its initial position at the initial epoch. This approximation compares well with true motion before shell crossing. Validity of this approximation can be used to infer that $\mathbf{u}(a, \mathbf{x}) \simeq \mathbf{g}(a, \mathbf{x})$ in the Zeldovich regime.

Zeldovich regime ends with formation of pancakes and shell crossing. After shell crossing particles oscillate about pancakes and form small clumps. These clumps move towards each other or have some bulk motion towards deep potential wells. Therefore in quasilinear regime velocities of particles are not aligned with gravitational force, except in direction of bulk motion of clump to which these belong.

The mismatch between velocity and force steadily increases till velocities are randomized inside clumps and dominate over any residual bulk motion. Such a situation is expected in highly nonlinear and large clusters that have either virialised or are close to it.

3 NEW STATISTICAL INDICATOR : VELOCITY CONTRAST

Above discussion shows that mismatch between velocity and gravitational force is a good indicator of nonlinearity in dynamics for pancake like models. However, it is as good an indicator for hierarchical models because nonlinearity in dynamics at small [mass] scales does not influence evolution of larger scales. *Shell crossing is necessary for formation of nonlinear objects at a given scale, independent of dynamical state of smaller scales.* Virialised structures can not form without shell crossing and mixing in the phase space. Merger of smaller structures leading to a larger virialised object is always accompanied by shell crossing at the new scale. Therefore, while studying a given mass scale we can neglect nonlinearity

in dynamics at much smaller scales. In fact numerical simulations of hierarchical models are based on the assumption that nonlinearity at small scales does not influence larger scales.

Mismatch between velocity and gravitational force is a vector quantity and is therefore difficult to handle and interpret. In addition it is a dimensional quantity and numerical value of the mismatch must be compared with something else for making a model independent estimate of the level of nonlinearity in dynamics. These considerations lead us to suggest the following form for velocity contrast :

$$D_{gu} \equiv \frac{(\mathbf{u} - \mathbf{g})^2}{u^2} \tag{5}$$

In this equation we can think of \mathbf{u} and \mathbf{g} as velocity of a given particle and force acting on it, respectively. Alternatively if smooth velocity and force fields are given, (5) defines a scalar field $D_{gu}(a, \mathbf{x})$. These two descriptions are equivalent for our purpose. If linear theory [or Zeldovich approximation] is valid for most particles [regions], then this quantity will be nearly zero for a large fraction of particles [mass]. With further evolution of clustering, more and more particles [mass] acquire significant values for this parameter. Regions containing particles [mass] with D_{gu} larger than a threshold will exhibit highly nonlinear dynamics and a study of these regions will offer insight into the study of nonlinear clustering. Luminous objects that we see have nonlinear density contrasts, therefore it is more meaningful to compare clustering properties of nonlinear objects in simulations with observations. D_{gu} provides a simple method for selecting nonlinear structures in a simulation.

This algorithm has two specific advantages over the method of density threshold or the friends of friends algorithm where one finds nonlinear structures by requiring local density to be higher than some cutoff or particles to be within some linking length of its nearest neighbour. Density threshold [linking length] for an object that has decoupled from expansion depends on the local symmetry of collapse, whereas deviations of velocity from acceleration depend only on the stage of dynamical evolution. When particles in a particular region are counted, in order to ascribe a density to that region, one does not take into account velocities of particles. A fast moving particle which is merely passing through a region will be counted in this process *even if it is following a Zeldovich trajectory with $\mathbf{u} = \mathbf{g}$* . In using D_{gu} as an indicator we exclude such particles until the alignment between \mathbf{u} and \mathbf{g} is disrupted. Our algorithm will select “nonlinear particles” in underdense regions as well. These are found in regions where pancakes are forming in otherwise underdense regions or where density is low but shear is important.

Velocity contrast suggests another method for studying approximation schemes. Note that D_{gu} directly characterises what could arguably be considered the most significant factor in formation of bound structures: *the ability of a local mass inhomogeneity to pull back particles towards it and thereby increase the local potential depth*. It is precisely the failure to do this which makes Zeldovich approximation break down at the onset of significant nonlinearity. For comparison, consider the “frozen potential approximation” [FPA hereafter; see Bagla and Padmanabhan (1994); also suggested independently by Brainerd, Scherrer and Villumsen (1993)] which may be thought of as a logical continuation of Zeldovich approximation: in ZA, velocities are frozen to initial values and force is ignored; in FPA, gravitational force is frozen to the initial value and the particles are moved in this given background potential. Studies have shown that FPA correctly reproduces the behaviour of particles near the mass concentrations since $(\mathbf{u} - \mathbf{g})$ is not pre-assigned to vanish in this approach. Therefore the structure of pancakes in FPA is similar to that in N-body simulations; pancakes do not thicken though they are not as thin as those seen in N-body simulations. Comparison of D_{gu} in FPA and N-body will be useful in understanding both.

Note that this statistical indicator takes into account both the velocity and force. It is possible to devise approximation schemes, like frozen flow (Matarrese et al 1992), adhesion model (Gurbatov, Saichev and Shandarin 1989), etc. which will move particles to the right regions but will give a physically unacceptable picture for the velocity field. In our opinion, approximation schemes should also provide correct velocity field if they have to offer insight into dynamics. D_{gu} may be used to discriminate between the dynamical content of different approximation schemes.

Velocity contrast can be used to compare analytical models with N-body. For simple analytic models of structure formation like spherical top hat it is possible to compute D_{gu} as a function of the density contrast δ . As we shall see this helps one in forming an intuitive picture of the nonlinear evolution.

4 N-BODY SIMULATIONS

To understand velocity contrast, we study it using N-Body simulations. Use of analytical methods for this study is made difficult by the fact that velocity contrast vanishes in linear regime. In this section we present results for two representative models of structure formation.

First model we consider is standard unbiased CDM normalized to COBE. Simulation of this model used a particle-mesh code on a 128^3 box with 128^3 particles. The size of the box in physical units is $90h^{-1}Mpc$. Figure 1 shows projected density field and velocity contrast field for slices $14h^{-1}Mpc$ thick. These slices corresponds to redshifts $Z = 3$, $Z = 1$ and $Z = 0$.

Comparison of panels at a given redshift shows that density and velocity contrast select almost the same set of nonlinear regions. These tend to disagree for some regions that appear dense to the eye but have not reached a sufficiently high level of nonlinearity in dynamics. On the other hand, some regions in what appears to be a void have a high value of velocity contrast. Highly nonlinear regions appear to have a larger radius of influence as diagnosed by velocity contrast, in comparison with density. This may indicate that velocity contrast does not increase substantially after virialisation, so that almost all members of a virialised cluster have similar values of velocity contrast even though density varies rapidly with distance from the centre. Evolution with redshift follows the expected pattern with more regions becoming nonlinear at later times.

Regions selected for contours of high velocity contrast tend to be spherical. This indicates that planar and filamentary structures can not attain a very high level of nonlinearity in dynamics — for nonspherical structures there is always some direction in which bulk velocity dominates over random motions.

An interesting feature that emerges from figure 1 is that velocity contrast filters out voids [apart from regions within them where large shear leads to formation of structures] more effectively as compared to density contrast.

The CDM model is a prime example of hierarchical clustering scenario with power at all scales and effective index varying from -3 to 1 . To see how this algorithm works in other cases, we studied the other extreme example. We considered a hypothetical universe which has power peaked at one dominant scale. The power spectrum for this model is taken to be

$$P(k) = \frac{A}{\Delta k (2\pi)^{1/2}} \exp \left[-\frac{(k - k_0)^2}{2(\Delta k)^2} \right] \quad (6)$$

with $k_0 = \pi/16$ and $\Delta k = \pi/64$. Clearly, this has power only in a band of width Δk peaked at k_0 . We chose $A = 68000$ so that the linearly extrapolated amplitude of the peak is unity at $Z \sim 2$, giving us sufficient coverage of both the linear and nonlinear regime. Our choice of k_0 and Δk ensures that the power is peaked at a large scale and it is concentrated in a very narrow range of scales. Note that this spectrum is somewhat similar to HDM models as far as the peak and smaller scales are concerned; standard HDM has $P(k) \propto k$ for small

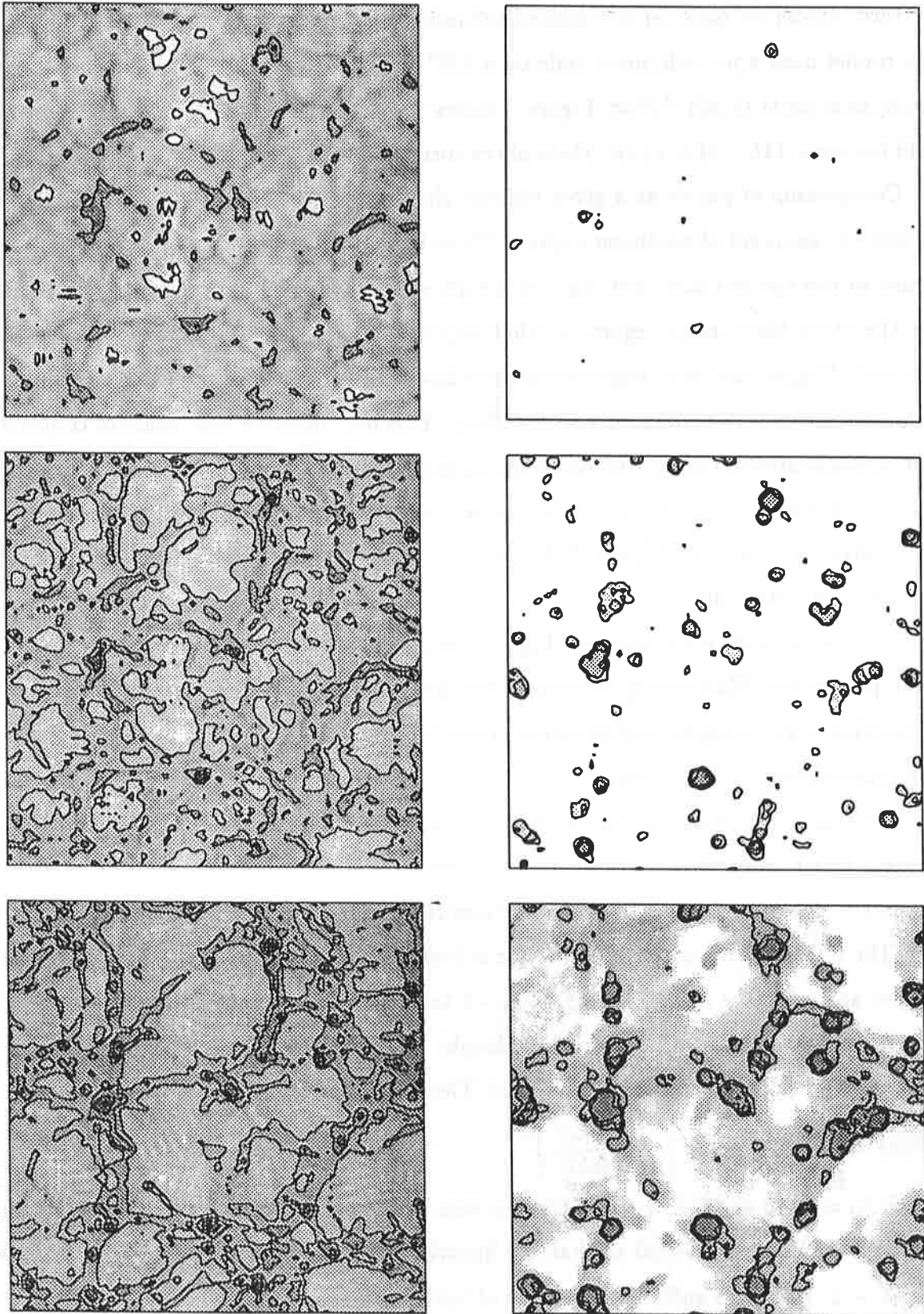


Figure 1. These figures show grey scale maps and contours of projected density and velocity contrast for slices taken from N-Body simulations of CDM. Left frames show the density field and right frames show velocity contrast field for the corresponding slices. Top frames are for $Z = 3$, middle frames are for $Z = 1$ and the bottom frames show the same slice at $Z = 0$.

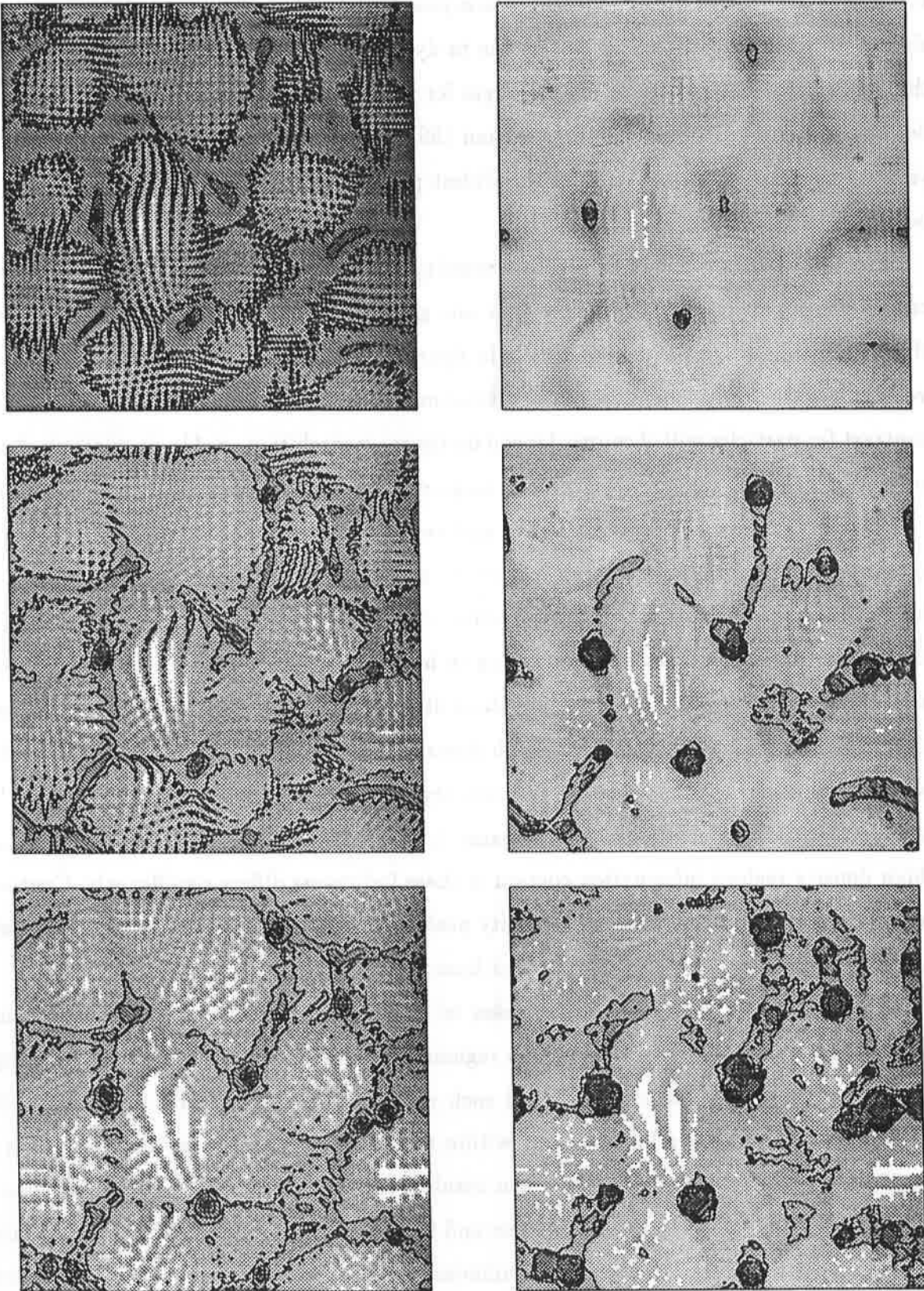


Figure 2. Same as figure 1 but for model with a gaussian power spectrum.

k but this model has an exponentially low power at small k . This is not very important since a k^4 spectrum will be generated due to dynamics (Zeldovich 1965). The evolution of this model provides an interesting paradigm for structure formation and will be discussed in detail elsewhere (Bagla and Padmanabhan 1995). Here we merely use this model to study velocity contrast so as to test it in the widest possible range. This simulation used a 128^3 box with 64^3 particles.

Figure 2 shows projected density and velocity contrast fields for this model. The thickness of the slice used here is $20L$, where L is one grid length in the simulation box. Panels of this figure follow the pattern of panels in figure 1, showing that the general behaviour of velocity contrast is independent of the type of model considered. Particular values of velocity contrast for particles will of course depend on the mass resolution used in simulations, but the smoothed field has same properties for a large range in mass scales : $M_{particle} \ll M \ll M_{box}$.

One key difference between density and velocity contrast is that density is a function of space and is same for particles located at same position whereas velocity contrast can be different for such particles. This feature of velocity contrast suggests that it can give us insight about some facets of clustering in highly nonlinear regions that are inaccessible through density contrast. We bring out these differences by studying some clusters in greater detail. Figure 3 shows close up of two rich clusters from the CDM simulation. For each cluster we have plotted projected density and velocity contrast fields for a cube of size $14h^{-1} Mpc$ centered at the cluster. Comparison of panels for density and velocity contrast shows that for high density regions information content of these indicators differs significantly. Contours of equal density indicate positions of density peaks and outlines of pancakes, whereas contours of velocity contrast show us regions that have significantly nonlinear dynamics.

Some regions that appear as pancakes or small density peaks are not seen in contours of velocity contrast, particles in these regions have not undergone any shell crossing but are only falling into the cluster. In all such regions, bulk flow towards the nearby cluster dominates over any random motions within the infalling mass. Many density peaks show complex substructure within. This can result from two scenarios : either there has been some recent merger of two small clusters and these have not mixed sufficiently or a group of particles with a much lower level of nonlinearity in dynamics has fallen into the cluster and it has not become an integral part of the cluster in dynamical sense.

Figure 4 shows a similar close up of a cluster for the model with gaussian power spectrum.

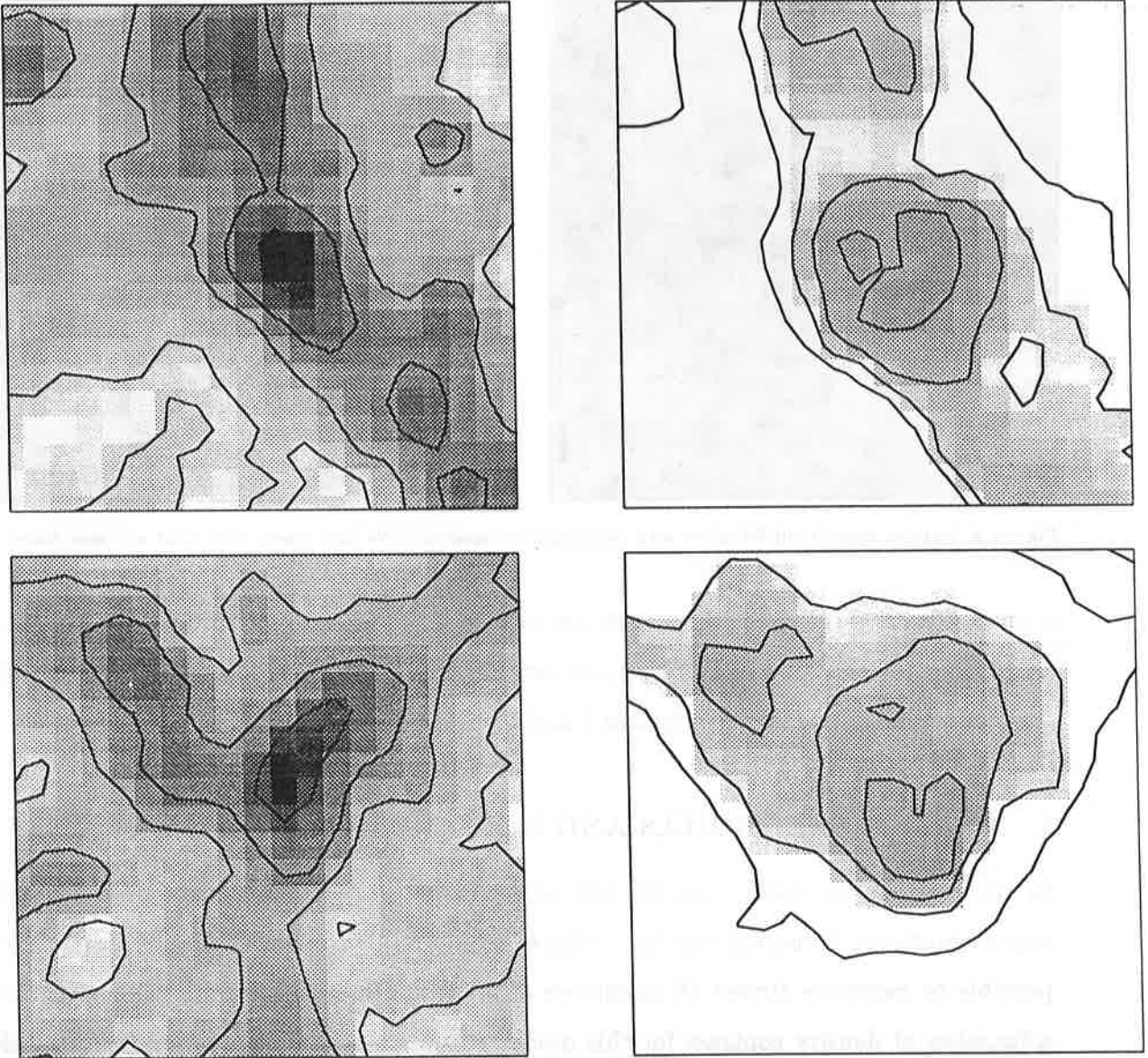


Figure 3. These figures show close up of two clusters for the CDM simulation. Left panels show projected density field and right panels show projected velocity contrast field. A cube of size $14h^{-1}Mpc$ centered at the clusters was used for these plots.

Here, the substructure is not as complex as in figure 3 as there was no small scale power in the initial spectrum. However, broad features are similar for both these models.

We now give the above results in a less picturesque manner. Figure 5 shows the fraction of particles with velocity contrast above a threshold as a function of threshold velocity contrast at different epochs for the CDM model. Same figure shows corresponding curves for the second model as dashed lines. For reference, we have labelled the equivalent density contrast for top hat spherical collapse on the top axis. These curves show that as clustering proceeds the fraction of particles with D_{gu} larger than a given threshold increases. Also, the fraction of particles selected with a high cutoff are significantly less than those selected by

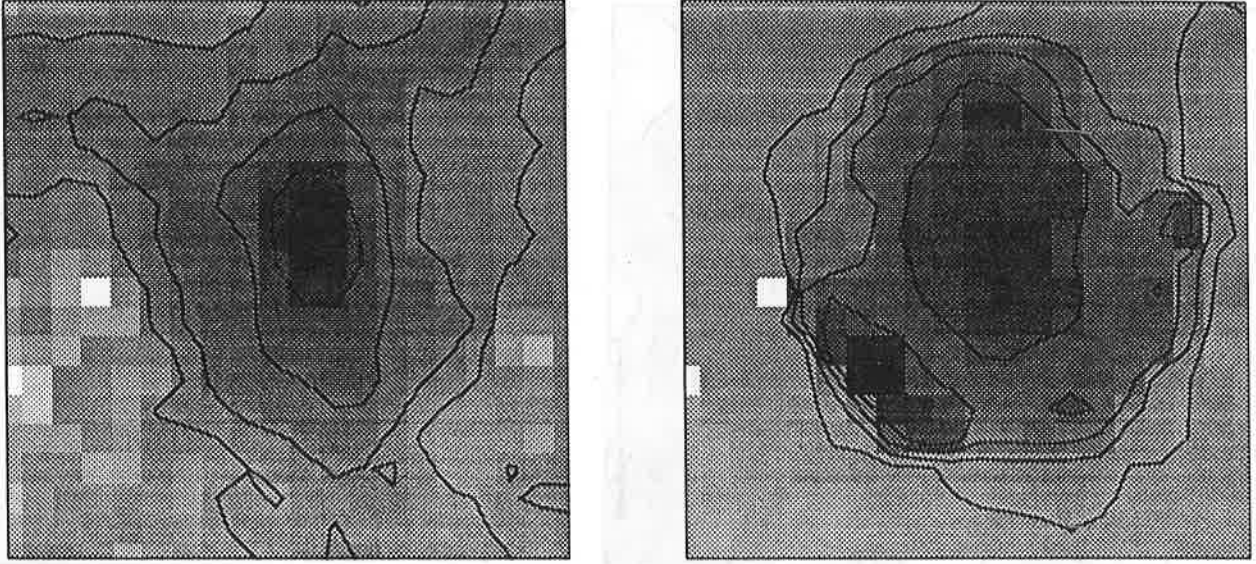


Figure 4. Same as figure 3 but for model with gaussian power spectrum. We have shown close up of only one cluster for this model.

a smaller value of D_{gu} . These features are expected in any indicator of nonlinearity and it is heartening to see that velocity contrast satisfies these criterion. These features can also be seen, at a qualitative level, in figures 1 and 2.

5 ANALYTICAL MODELS AND NONLINEAR APPROXIMATIONS

In this section we study velocity contrast with help of nonlinear models and analytical approximations. Spherical top hat collapse is one model of nonlinear collapse where it is possible to calculate almost all quantities of interest. Here we compute velocity contrast as a function of density contrast for this model. Initial velocities are related to initial density contrast through the potential as

$$\begin{aligned} \mathbf{u}(a, \mathbf{x}) &= \mathbf{g}(a, \mathbf{x}) = -\nabla\psi(a, \mathbf{x}) \\ \nabla^2\psi(a, \mathbf{x}) &= \frac{\delta(a)}{a} \end{aligned} \quad (7)$$

Here \mathbf{x} is the comoving coordinate and relates to the proper coordinate \mathbf{r} in the usual way. These initial conditions put the system into growing mode and this leads to the following solution.

$$\begin{aligned} r &= \frac{r_{max}}{2} (1 - \cos \theta) \\ a &= \frac{3a_i}{5\delta_i} \left[\frac{3}{4} (1 + \delta_i) (\theta - \sin \theta) \right]^{2/3} \\ \delta &= \frac{9 (\theta - \sin \theta)^2}{2 (1 - \cos \theta)^3} - 1 \end{aligned} \quad (8)$$

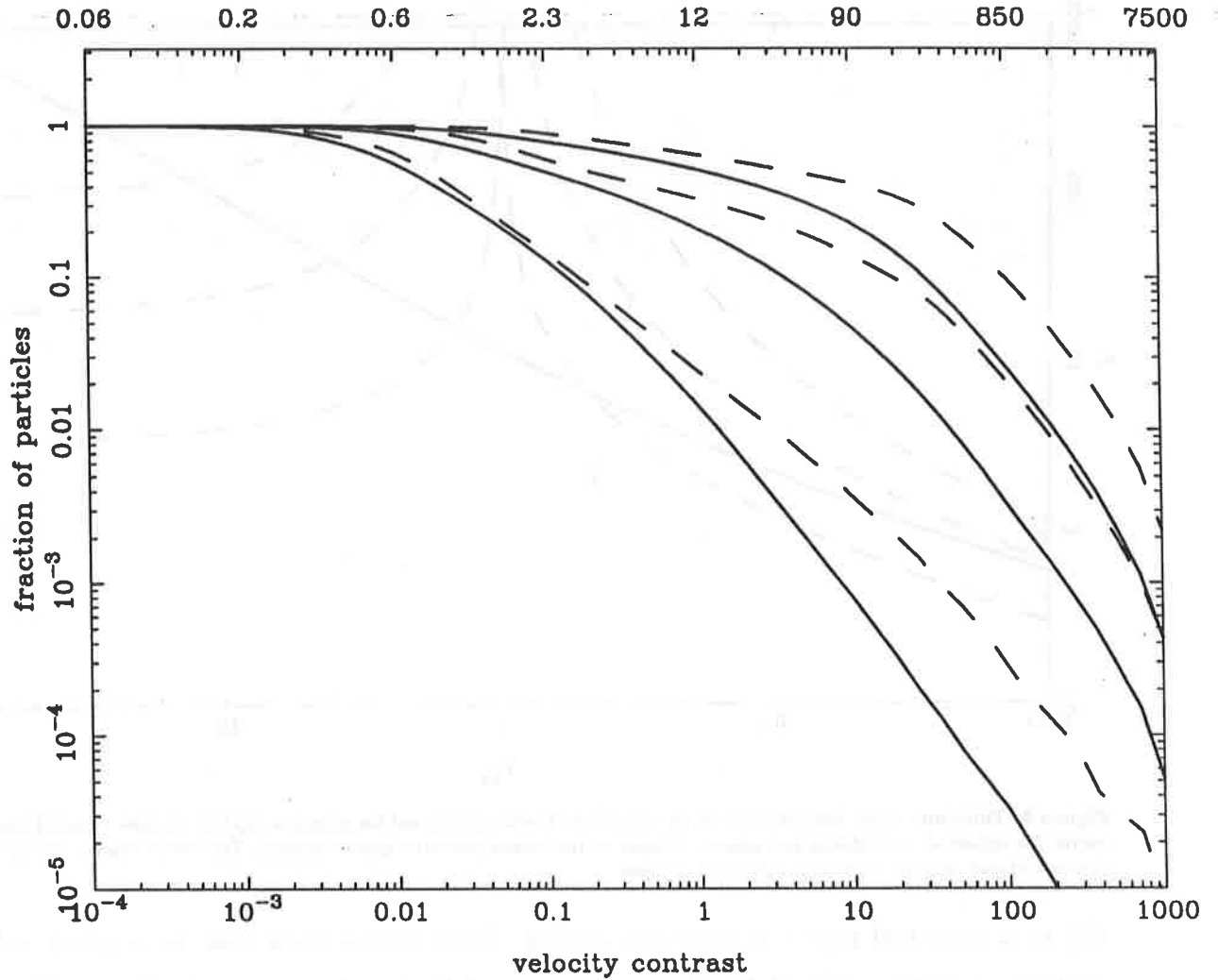


Figure 5. Fraction of particles above a threshold velocity contrast are shown as a function of threshold for three redshifts : $Z = 3, 1$ and 0 . Thick lines are for CDM and dashed lines are for model with gaussian power spectrum. Top axis has been labelled by the equivalent density contrast for spherical top hat collapse.

We can also write down expressions for \mathbf{g} and \mathbf{u} , leading to an expression for velocity contrast.

$$\begin{aligned} \mathbf{g} &= -\frac{\delta}{3a^2}\mathbf{r} \\ \mathbf{u} &= -\frac{1}{3a}\frac{\partial \ln(1+\delta)}{\partial a}\mathbf{r} \end{aligned} \quad (9)$$

From these, given a value of velocity contrast we can determine the corresponding phase angle and solve for density contrast. In figure 6 we have plotted density contrast as a function of velocity contrast for this model.

One certainly does not expect STH to be a good model for generic nonlinear collapse and it is worthwhile to consider evolution of velocity contrast for symmetric collapse in other approximations. In figure 6 we have also plotted curves computed using FPA for one, two and three dimensional models; that is, in each case we solve for particle trajectory around the potential produced by a sheet [1-D motion, sheet is 2D], filament [2D motion, source is

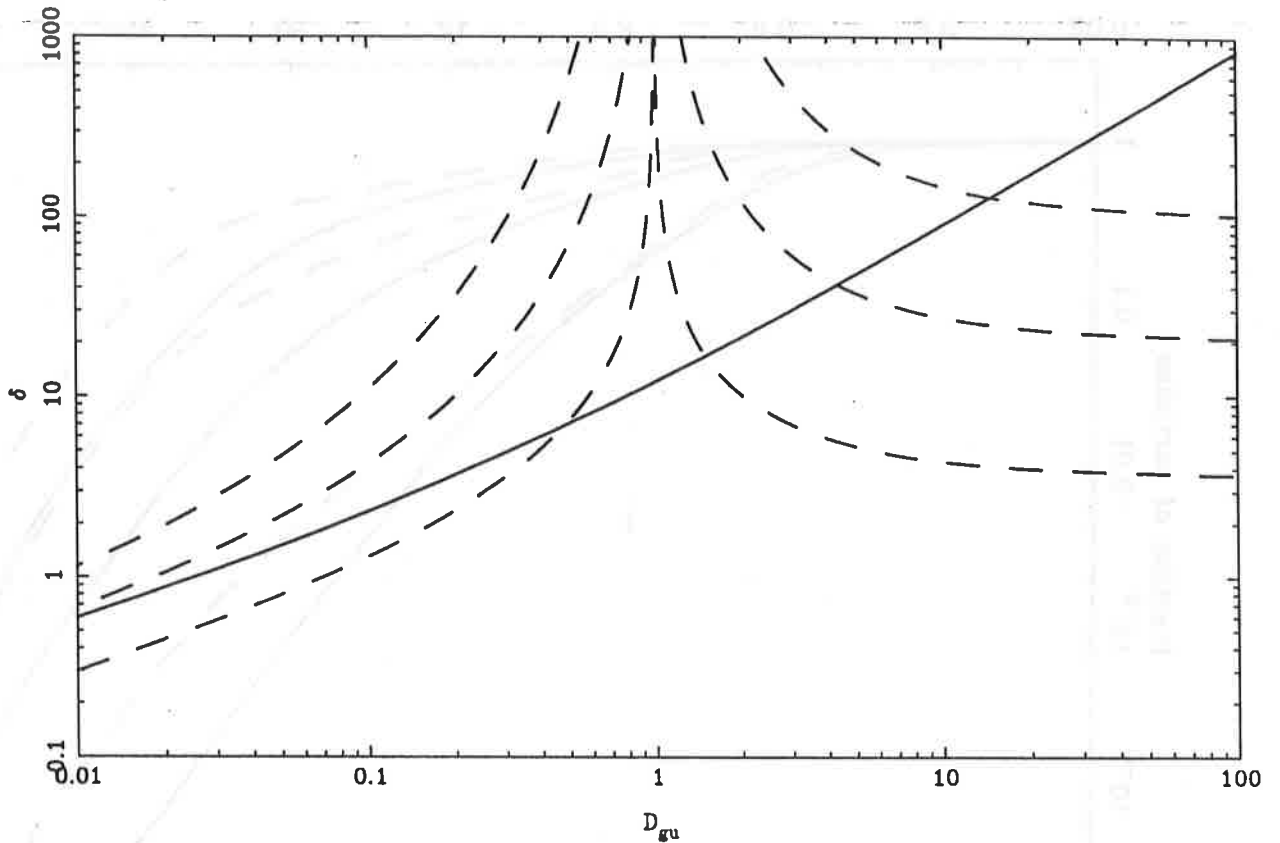


Figure 6. Thick line shows density contrast as a function of velocity contrast for spherical top hat collapse. Dashed lines show curves for spherical, cylindrical and planar collapse in the frozen potential approximation. The lowest curve corresponds to planar collapse and the highest to spherical collapse.

1D] or a spherical region of constant density. These curves show that for a given velocity contrast, density is lowest for planar collapse and highest for spherical collapse. The ratio of densities for $D_{gu} = .1$ is 1 : 3.2 : 8.9. This clearly shows that velocity contrast is a better algorithm for selecting nonlinear regions as it defines nonlinearity as deviations from trajectories in the linear regime. It is clear that a density threshold for selecting nonlinear structures will either select spherical objects that have not turned around or shell crossed, or it will miss out mildly nonlinear planar structures. Another feature that is seen in these graphs is that after shell crossing, density decreases while velocity contrast increases. When the particle turns back towards the pancake, it is possible for it to return to very small values of D_{gu} but this happens only because in FPA we are using the initial gravitational force. In exact evolution, g evolves sufficiently to rule out small values of D_{gu} . Another feature that is seen here is that shell crossing occurs in FPA at $D_{gu} = 1$ as acceleration vanishes at the point where pancake is formed. [In FPA we use initial acceleration, which vanishes at the caustic in symmetric cases. In a general case, there will be some residual acceleration along the caustic.]

Velocity contrast can be studied within the framework of adhesion model (Gurbatov, Saichev and Shandarin 1989). In this model the equation of motion is modified to include an ad hoc viscous term that ensures thin pancakes. The equation of motion is

$$\frac{\partial \mathbf{u}}{\partial a} + (\mathbf{u} \cdot \nabla) \mathbf{u} = \nu \nabla^2 \mathbf{u} \quad (10)$$

A comparison with (1) shows that viscosity term tries to mimic gravitational force, and

$$\mathbf{g}_{eff} = \mathbf{u} + \frac{2b}{3Q} \nu \nabla^2 \mathbf{u} \quad (11)$$

In this equation, gravitational force is some kind of an effective acceleration modelled by the viscosity term.

The general solution to (10) is well known and it allows us to compute \mathbf{u} for any particle, given the initial velocity potential. We can use this solution to compute velocity contrast, for the effective force in adhesion model. It is apparent that D_{gu} is significantly large only at the caustics in the limit $\nu = 0$. At present we are studying D_{gu} as a function of ν , which could lead to an understanding of the origin of effective viscosity in the adhesion model.

6 EVOLUTION AND CLUSTERING OF NONLINEAR STRUCTURES

Velocity contrast and its relation with density contrast is shown in figure 7 where we have plotted contours of equal population on the $(1 + \delta) - D_{gu}$ plane. This plot shows contours for two epochs each for the two models we are using in this paper : CDM and gaussian power spectrum. For comparison we have also plotted the curve obtained from STH on each of the panels. These plots show that there is an average relation between velocity contrast and density that is independent of epoch and model, and holds for a large range of scales. For CDM simulations, it is apparent that the relation evolves at high velocity contrast and the density for a given velocity contrast increases with time. This could imply a shift from mostly planar collapse occuring at early epochs towards more instances of spherical collapse at later stages.

There is a large dispersion about the average relation between density and velocity contrast. Part of this dispersion arises from the fact that collapse of various kinds, from planar to spherical, is occuring in the simulation volume. As indicated by relation of velocity contrast with density for symmetric collapse in FPA, the variation in density contrast for a given velocity contrast may be as large as an order of magnitude. Contours for the second

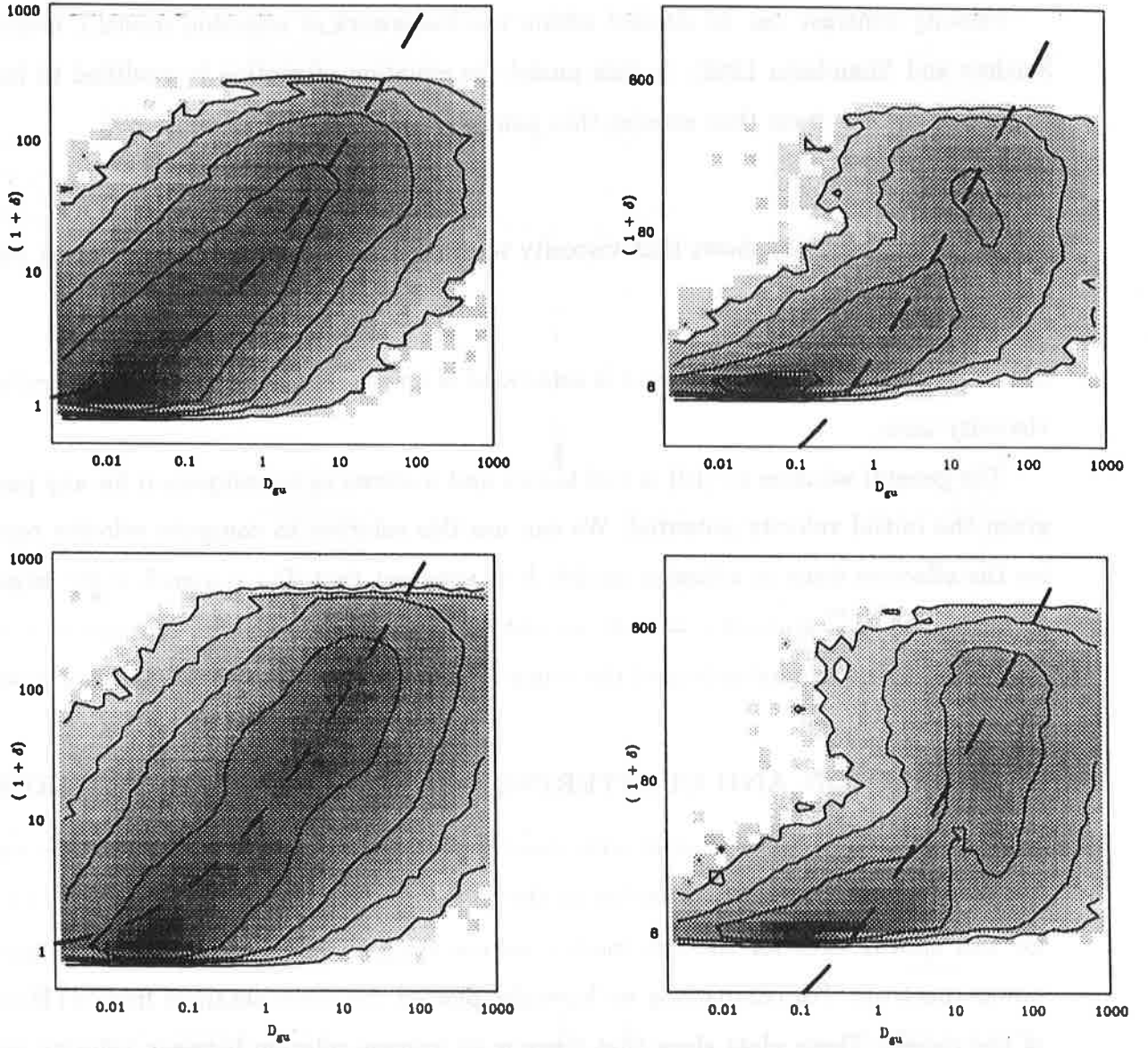


Figure 7. Contours of equal population on the density – velocity contrast plane. Left panels show these contours for CDM and right panels are for model with gaussian power spectrum. Top panels are for $Z = 1$ and bottom panel is for $Z = 0$. Dashed line in each panel shows relation for STH collapse.

model show a very large dispersion at large velocity contrast. This indicates ongoing collapse of objects with different local symmetries.

Velocity contrast is a good indicator of nonlinearity. In a simulation output we can identify nonlinear regions by requiring velocity contrast to be higher than some threshold. Regions selected in this manner will in general have clustering properties that differ from those of the total underlying mass. We study clustering properties of these regions and define a scale dependent bias parameter. Only those regions where particles have undergone shell crossing [at the scale of a galaxy] can we form virialised structures like galaxies that we see. Therefore, the clustering properties of regions with velocity contrast above a threshold are

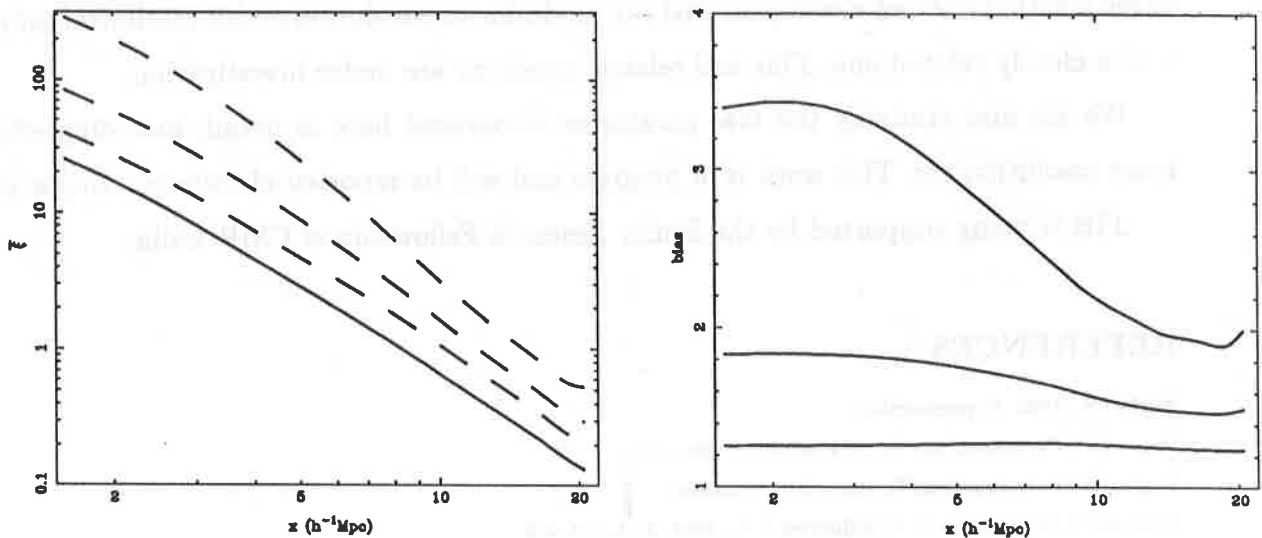


Figure 8. $\bar{\xi}$ vs. x for CDM at $Z = 0$. We have also plotted $\bar{\xi}$ for particles with $D_{gu} > .1, 1$ and 17 . Left panel shows bias parameter for these threshold values as a function of scale.

essentially clustering properties of regions that can host visible structures. Figure 8 shows averaged correlation function for the underlying mass and also for regions with velocity contrast above a threshold in a CDM simulation at $Z=0$. Threshold values used here were $0.1, 1$ and 17 . The averaged correlation function $\bar{\xi}$ and bias b are defined here as :

$$\bar{\xi}(a, x) = \frac{3}{x^3} \int_0^x \xi(a, y) y^2 dy$$

$$b^2(x) = \frac{\bar{\xi}(x; D_{gu} > D_{guc})}{\bar{\xi}(x; \text{all particles})} \quad (12)$$

where ξ is the two point correlation function. The relative bias decreases with the scale, approaching unity at very large scales, and increases with the cutoff used in selecting particles. This scale dependent bias may be used in understanding relative bias between different kinds of objects, like different populations of galaxies and clusters of galaxies. Unlike the method of peaks in the initial distribution, the algorithm described in this paper clearly picks out regions that are dynamically “nonlinear” and therefore are potential sites for galaxy formation. It may be possible to model the environmental effects in galaxy formation as D_{gu} describes the level of “churning” for nonlinear regions which is likely to be an important factor.

7 CONCLUSIONS

The purpose of this note was to introduce this new statistical parameter, study its behaviour and establish a prima facie case that it is worth being considered further. It will be interesting

to see whether one can develop an analytic model for the evolution of this statistical indicator – or a closely related one. This and related questions are under investigation.

We are also studying the bias parameter introduced here in detail, including effect of mass resolution etc. This work is in progress and will be reported elsewhere (Bagla 1995).

JSB is being supported by the Senior Research Fellowship of CSIR India.

REFERENCES

- Bagla J.S., 1995, In preparation
Bagla J.S., Padmanabhan T., 1994, MNRAS, 266, 227
Bagla J.S., Padmanabhan T., 1995, In preparation
Brainerd T.G., Scherrer R.J., Villumsen J.V., 1993, ApJ, 418, 570
Bertschinger E., Gelb J.M., 1991, Computers in Physics, 5, 164
Gurbatov S.N., Saichev A.I., Shandarin S.F., 1989, MNRAS, 236, 385
Matarrese S., Lucchin F., Moscardini L., Saez D., 1992, MNRAS, 259, 437
Zeldovich Ya.B., 1965, Adv. Astron. Astrophys., 3, 241 (§§4, 10, 24, 28)
Zeldovich Ya. B., 1970, A&A, 5, 84